Opto-vTrap, an optogenetic trap for reversible inhibition of vesicular release, synaptic transmission and behavior

Joungha Won[1,2], Yuriy Pankratov[3], Minwoo Wendy Jang[1,4], Sunpil Kim[1,4], Yeon Ha Ju[1], Sangkyu Lee[1], Seung Eun Lee[5], Arie Kim[1], Soowon Park[1], C. Justin Lee[1,4,*] and Won Do Heo[1,2,*]

[1] Center for Cognition and Sociality, Institute for Basic Science (IBS), Daejeon, Republic of Korea

[2] Department of Biological Sciences, Korea Advanced Institute of Science and Technology (KAIST), Daejeon, Republic of Korea

[3] School of Life Sciences, University of Warwick, Coventry, CV4 7AL, United Kingdom

[4] KU-KIST Graduate School of Converging Science and Technology, Korea University, Seoul 02841, Republic of Korea

[5] Virus Facility, Research Animal Resource Center, Korea Institute of Science and Technology (KIST), Seoul 02792

*Correspondence to C. Justin Lee (cjl@ibs.re.kr) and Won Do Heo (wondo@kaist.ac.kr)

Abstract

Spatiotemporal control of brain activity by optogenetics has emerged as an essential tool to study brain function. For silencing the brain activity, optogenetic probes, such as halorhodopsin and Archaerhodopsin, inhibit transmitter release indirectly by hyperpolarizing the membrane potentials. However, those probes cause undesirable ionic imbalance and rebound spikes. Moreover, they are not applicable to use in non-excitable glial cells. Here, we engineered Opto-vTrap, a light-inducible and reversible inhibition system to temporarily trap the transmitter-containing vesicles from exocytotic release. Light-activation of Opto-vTrap caused a full vesicle-clusterization and complete inhibition of exocytosis within one minute, which recovered within 30 minutes after light-off. We found a

significant reduction of synaptic- and glio-transmission upon activation of Opto-vTrap in acute brain slices. Opto-vTrap significantly inhibited hippocampus-dependent memory retrieval with a full recovery within an hour. We propose the Opto-vTrap as a next-generation optogenetic silencer to control brain activity and behavior with minimal confounding effects.

Introduction

Understanding the brain circuits which are activated or silenced by releasing and receiving the molecules between brain cells is a major challenge to neuroscience. During the fast-functional information transfer between neuron and neuron, or glia and neuron, the transmitters are released by calcium-triggered vesicular exocytosis (Harada et al., 2015; Parpura and Zorec, 2010; Sudhof, 2012). There has been a considerable research effort on developing tools for modulating brain activity from cellular level to behaving animal. To spatially, temporally, and cell-type specifically modulate brain circuits, optogenetic strategies have emerged. Light-gated cation channel, channelrhodopsin-2 (ChR2), is widely used for stimulating brain networks by depolarizing membrane potential followed by light illumination (Boyden et al., 2005; Lin et al., 2009; Nagel et al., 2003). Activated ChR2 increases calcium influx through the gate of ChR2 and voltage-gated calcium channel, and it causes the release of transmitters (Schoenenberger et al., 2011). Optogenetic tools for stimulating neuronal activity, such as ChR2, ChR2 variant, or other similar, typically utilize cation channels that depolarize membrane potential (Nagel *et al.*, 2003).

Meanwhile, optogenetic tools for inhibiting neuronal activity, such as halorhodopsin (NpHR), archaerhodopsin (Arch) and anion-conducting channelrhodopsin have become popular. NpHR and Arch utilize light-inducible chloride or proton pump that hyperpolarize membrane potential (Chow et al., 2010; Zhang et al., 2007). Although light-activation of NpHR and Arch efficiently silence neuronal activity within a short time scale, a prolonged activation results in critically confounding responses (Wiegert et al., 2017). For instance, prolonged activation of NpHR causes an accumulation of intracellular chloride ions and $GABA_A$ reversal potential shift, which results in inadvertent excitatory responses to GABA (Raimondo et al., 2012). In addition, NpHR-mediated hyperpolarization causes recovery from inactivation of the low-voltage-activated T-type calcium channels, which are subsequently activated upon light-off, resulting in an unintended burst firing (Mahn et al., 2016; Mattingly et al., 2018; Weiss et al., 2012). Furthermore, activation of Arch causes a decrease in intracellular proton concentration or high pH, which has a profound effect on various cellular pathways, such as an increase in calcium concentration and neurotransmitter release

(Mahn *et al.*, 2016). Due to these critical issues, many researchers have turned away from NpHR and Arch and started to prefer chemogenetic approaches, such as Gi-Designer Receptors Exclusively Activated by Designer Drugs, (G_i-DREADD) (Armbruster et al., 2007). However, G_i-DREADD also suffers from the same issue of unintended burst firing upon activation, in addition to other disadvantages such as slow drug onset and offset kinetics (Saloman et al., 2016; Wiegert *et al.*, 2017). Lastly, NpHR and Arch are not applicable in non-excitable glial cells, such as astrocyte. Due to these shortcomings, there is a pressing need for developing advanced optogenetic silencers without affecting membrane potential.

To circumvent the shortcomings of manipulating membrane potential, optogenetic and chemogenetic tools that directly target and disrupt the synaptic vesicular release machinery has been considered (Karpova et al., 2005; Lin et al., 2013; Liu et al., 2019). The synaptic vesicle release machinery includes Soluble N-ethylmaleimide-sensitive fusion Attachment protein REceptor (SNARE) complex-mediated vesicle docking and priming, complexin binding to SNARE complex, and calcium-binding to synaptotagmin-1 and zippering SNARE complex to form a pore for vesicle fusion (Rizo and Xu, 2015; Sudhof, 2004; Zhou et al., 2017). The SNARE complex is composed of the highly-conserved vesicular SNARE (v-SNARE), including VAMP2(Synaptobrevin2), and the target plasma membrane SNARE (t-SNARE), including syntaxin-1 and SNAP25 (Sollner et al., 1993). To optogenetically target and disrupt vesicular release machinery, Lin et al introduced Chromophore-assisted light inactivation (CALI)-based synaptic inhibition (InSynC) (Lin, Sann et al. 2013). This system utilizes a light-dependent generation of singlet oxygen that damages v-SNARE and disrupts the synaptic vesicle release. However, this system has a serious off-target effect, because the generated singlet oxygens can diffuse and permanently destroy nearby proteins. Recently reported photo-activable botulinum neurotoxin (PA-BoNT) tried to overcome this limitation by directly cleaving VAMP2 upon light-illumination (Liu *et al.*, 2019). However, this PA-BoNT showed a very long recovery time of about 24 hours in *C. elegans* possibly because it takes a long time for the cleaved VAMP2 to be replenished either by *de novo* protein synthesis or by lateral trafficking from undamaged VAMP2 (Liu *et al.*, 2019). InSynC has a similar long recovery time due to the slow

replenishing of the damaged proteins. The long recovery time usually imposes a time-constraint on the type of experiments that can be performed: For example, short-duration behavioral tests such as novel object recognition, object place recognition, five-trial social interaction, and fear conditioning and extinction cannot be performed with an optogenetic tool having 24-hour recovery time. Therefore, it is necessary to develop a novel optogenetic tool that disrupts vesicular release machinery at a fast recovery time.

In response to the growing need, we have designed and developed Opto-vTrap, a fast-reversible optogenetic inhibition system for direct inhibition of vesicular exocytosis. This system directly targeting and sequestering transmitter-containing vesicle into the vesicle cluster and inhibit vesicular release. Unlike the Gi-DREAD system, Opto-vTrap quickly activates and recovers by using light-inducible on and off. Unlike the NpHR or Arch, this system does not induce membrane potential change. And Opto-vTrap has a much faster recovery than the other vesicle targeting optogenetic probes. We employed the recently characterized LARIAT (light-activated reversible inhibition by assembled trap) (Lee et al., 2014) to directly target and reversibly disrupt the vesicular release machinery. LARIAT utilizes the property of blue light-inducible heteromerization between cryptochrome 2 (CRY2) from *Arabidopsis thaliana* and cryptochrome-interacting basic helix-loop-helix 1 (CIB1), which has sub-second time resolution and fast reversibility within minutes (Kennedy et al., 2010). With this property, LARIAT sequesters a target protein by forming a CRY2-CIB1 multimeric complex (Kennedy *et al.*, 2010; Lee *et al.*, 2014). Here we show that Opto-vTrap effectively and reversibly traps synaptic vesicles in neurons as well as gliotransmitter-containing vesicles in astrocytes. We further show that Opto-vTrap can be widely used in cells, brain slices, and animal behavioral experiments, with recovering at a fast time course and without affecting membrane potential.

Result

Engineering Opto-vTrap, a LARIAT-based vesicle-trapping system

To directly target and reversibly disrupt the vesicular release machinery, we newly designed Opto-vTrap, a light-inducible vesicle-trapping system based on LARIAT (Figure 1A). LARIAT is composed of two critical components: the light-responsive CRY2 and its target protein, CIB1, which is conjugated with a multimeric protein of interest (Figure 1A). CRY2 reversibly and strongly interacts with CIB1 to form a CRY2:CIB1 heterodimer and clusters with other CRY2s' (CRY2:CRY2) to form homomeric oligomers upon blue light illumination (Bugaj et al., 2013; Rosenfeldt et al., 2008). To increase the efficiency of light-induced vesicle trapping through heteromeric dimer- and homomeric oligomer-formation, we tried to reduce the size of CIB1 and CRY2; we utilized the shortened versions of N-terminal photolyase homology region (PHR) domain (amino acid 1-498) of CRY2 and C-terminal truncated version (amino acid 1-170) of CIB1 (CIBN) (Kennedy *et al.*, 2010) (Figure 1A) (Hereafter, CRY2 denotes this shortened version of PHR domain (amino acids 1–498) of CRY2). To optically trap vesicles, we conjugated CIBN with the v-SNARE protein, VAMP2 (Figure 1A), which interacts with the t-SNARE proteins such as SNAP25 and syntaxin-1 (Hastoy et al., 2017; Hayashi et al., 1994; Lin *et al.*, 2013; Schoch et al., 2001). As a fluorescent reporter, we inserted mCherry in between CIBN and VAMP2 (Figure 1A) because it has been shown that tagging a fluorescent protein to cytosolic N-terminus or lumenal C-terminus of VAMP2 does not interfere with VAMP2 function during exocytosis (Deak et al., 2006). For CRY2, we conjugated it with mCitrine as a fluorescent reporter (Figure 1A). Thus, Opto-vTrap was composed of two molecular components in the over-expression vector (pcDNA3.1) each containing CMV::CIBN-mCherry-VAMP2 (CIBN-VAMP2) and CMV::CRY2PHR-mCitrine (CRY2) (Figure 1A). Upon blue light (~488 nm) illumination of Opto-vTrap, CRY2 responds by forming heteromeric dimers of CRY2:CIBN-VAMP2 and homomeric oligomers of CRY2:CRY2 (Figure 1B).

To visualize and test whether Opto-vTrap clusters intracellular vesicles upon light-stimulation, we co-expressed CIBN-VAMP2 and CRY2 in Cos-7 cells and measured the movement

of vesicles. We used a blue-laser to stimulate Opto-vTrap and examined the clustering of vesicles under confocal microscopy (Figure 2B). Before blue-light illumination, CIBN-VAMP2 and CRY2 signals were diffusely distributed in the cytosol (Figure 2B, left panel and 2I-J). However, upon illumination of blue-laser at 0.2 Hz and 20% duty cycle (1 s exposure, 4 s off, at 5 s interval), we observed a simultaneous clustering of both CIBN-VAMP2 and CRY2 within 5 minutes and throughout the light illumination, which fully recovered 15 minutes after laser-off (Figure 2B). The time course of the line-intensity image along the yellow arrow in Figure 2B showed a detailed time course of the CIBN-VAMP2 and CRY2 clustering and recovery (Figure 2C and 2D). We observed an immediate clustering within two minutes and a much slower declustering, which took about 15 minutes to fully recover (Figure 2D). We also observed that the relative number of CIBN-VAMP2 puncta was increased within two minutes of laser-on (Figure 2E-G) and slowly recovered after 15 minutes of laser-off (Figure 2E-G). To determine the time course of the clustering between CIBN-VAMP2 and CRY2, we calculated the Pearson's correlation coefficient at each time point and found that the value of coefficient steeply increased with a time constant of $\tau = 10.9$ s, and plateaued after 60 s (Figure 2H) and exponentially decreased with $\tau = 543.9$ s (Figure 2J). These results indicate that the two components of Opto-vTrap quickly cluster within 1 or 2 min upon light stimulation and recover slowly within 15 min after stimulation-off.

Opto-vTrap impaired vesicular exocytosis

To examine whether Opto-vTrap impairs vesicular exocytosis upon light-stimulation, we performed TIRF (total internal reflection fluorescence)-imaging to visualize individual exocytotic events (Becherer et al., 2007). To visualize exocytotic events, we expressed Opto-vTrap in Neuroscreen-1 (NS-1) cells together with NPY-VENUS, neuropeptide-Y (NPY) tagged with VENUS pH-insensitive fluorescent protein (Figure 3A). To induce exocytosis, we applied high potassium solution (70 mM KCl) at 30 s after the start of 488 nm blue light stimulation at 5 Hz and 40% duty cycle (80 ms exposure, 120 ms off, at 200ms interval) (Figure 3B). The 488nm laser simultaneously activated Opto-vTrap and visualized NPY-VENUS under TIRF imaging (Figure 3B). We observed

that in the control condition (without CRY2), we observed numerous spots of about 1 μm size appear upon high potassium application, which were totally absent in the Opto-vTrap condition (Figure 3C and 3D), indicating that light-stimulation of Opto-vTrap abolished exocytosis of NPY-VENUS containing vesicles. Detailed analysis of each exocytotic event measured by fluorescence intensity (Figure 3D) showed that KCl-induced exocytotic events occur quickly after KCl application in the control condition but not in the Opto-vTrap condition (Figure 3E). The peak amplitude fluorescence intensity during exocytosis was completely eliminated by light stimulation of Opto-vTrap (Figure 3F). These results indicate that Opto-vTrap effective block vesicular exocytosis.

Activation of Opto-vTrap does not affect membrane potential

To examine whether Opto-vTrap activation affects membrane potential, we constructed a lentiviral Opto-vTrap vector containing CRY2PHR-P2A-CIBN-mCherry-VAMP2 under CamKIIα promoter and bi-laterally injected the lentivirus into the CA3 hippocampus (Figure 4A). We then recorded membrane potential changes in Opto-vTrap-expressing CA3 pyramidal neurons of the acutely prepared hippocampal slices with current steps ranging from -100 pA to +40 pA (Figure 4B). Immediately after current steps, we measured changes in membrane potential upon continuous blue-light stimulation onto the CA3 region (Figure 4C). We observed that continuous blue-light illumination for 10 minutes did not cause any membrane potential change (Figure 4C and 4D). These results indicate that activation of Opto-vTrap does not affect membrane potential.

Activation of Opto-vTrap inhibits evoked EPSC in Schaffer-collateral synapses

To test whether activation of Opto-vTrap can selectively inhibit synaptic transmission in Schaffer-collateral synapses, we recorded evoked excitatory post-synaptic currents (eEPSCs) from CA1 pyramidal neurons while electrically stimulating the Schaffer-collateral pathway (Amaral and Witter, 1989) with a paired-pulse electrical stimulation (Figure 4E). After establishing a stable baseline of the eEPSC amplitude, we turned on a continuous 300 μW of continuous blue-light onto the CA1 region, near the patch clamped cell (Figure 4E). We observed that in control condition

without virus injection, light-stimulation did not cause any changes in eEPSC of the 1st eEPSC, or 2nd eEPSC, or paired-pulse ratio (Figure 4F-L), suggesting no detrimental effect of light-illumination on synaptic transmission. In addition, there was no significant difference between control and Opto-vTrap expressing group in evoked-EPSC amplitude, mEPSC amplitude and frequency before light illumination (Figure 4F and Figure S4 A-D). Meanwhile, there was no significant difference between control and Opto-vTrap expressing group in action potential firing frequency during current injection, AP threshold, and input resistance (Figure S1). **Furthermore, biogenesis of vesicle and presynaptic volume was not affected by Opto-vTrap expression (Figure S2).** These results indicate that overexpression of Opto-vTrap has no activity in the absence of light stimulation. In contrast, Opto-vTrap-injected condition showed a significant reduction of 1st eEPSC amplitude and 2nd eEPSC amplitude after 15 min of light-on (Figure 4G-J). In addition, we further constructed AAV Opto-vTrap under CK(0.4) promoter which is a short version (0.4 kb) of CamKIIa promoter (8.5 kb) (Dittgen et al., 2004) and tested in Schaffer collateral synapses (Figure S5 A). We observed about 50% reduction of both 1st and 2nd eEPSC amplitude within 10 min of light-on (Figure S5 B-F). AAV-Opto-vTrap improved about 5% of inhibition efficiency and about 5 min of onset speed over lentiviral Opto-vTrap. In addition to evoked-EPSC, the frequency of mEPSC was reduced after 15 min of light-on in Opto-vTrap-injected condition (Figure S4). And both the 1st and 2nd amplitudes were fully recovered within 30 min after light-off (Figure 4G-J). These results indicate that Opto-vTrap can effectively and reversibly inhibit neurotransmitter release in the brain circuit. Interestingly, activation of Opto-vTrap did not change the paired-pulse ratio (PPR) (Figure 4K and 4L), which is a conventional marker for changes in presynaptic release probability (Dobrunz and Stevens, 1997). One of the factors that induces changes in PPR is a change in residual Ca^{2+} in the presynaptic terminal (Dobrunz and Stevens, 1997). Therefore, no change in PPR (Figure 4K and 4L) suggests that inhibition of vesicular release by Opto-vTrap may not influence presynaptic residual Ca^{2+}.

Activation of Opto-vTrap inhibits neocortical astrocytic vesicular gliotransmitter release

To test whether Opto-vTrap can selectively inhibit vesicular release in non-excitable cells such as astrocytes, we constructed lentiviral vector containing Opto-vTrap, CRY2PHR-P2A-CIBN-mCherry-VAMP2, under compact GFAP promoter, GfaABC1D (Lee et al., 2008) and injected lentivirus into layer 2/3 of the neocortex (hereafter, GFAP promoter denotes GfaABC1D promoter) (Figure 5A). We recorded NMDA receptor (NMDAR)-mediated spontaneous current activities in layer 2/3 neurons that were nearby the Opto-vTrap expressing astrocytes in acutely prepared cortical slices (Figure 5A). To selectively activate astrocytes we applied TFLLR, a selective agonist of PAR1, which is a G_i- and G_q-coupled GPCR which causes Ca^{2+} increase in astrocytes (Hollenberg et al., 1997). It has been demonstrated that PAR1 activation induces both TREK-1-mediated fast and Best1-mediated slow glutamate releases in hippocampus CA1 (Woo et al., 2012). In cortical layer 2/3 neurons, we found three types of NMDAR-mediated spontaneous transient inward currents, characterized by the decay time kinetics: neuronal mEPSC with decay time of 20 ms and marked as blue circles, glial-induced fast current (gFICs) with decay time of 40-45 ms and marked as orange squares, and glial-induced slow current (sFICs) with decay time of 100-300 ms and marked as green triangles (Figure 5B and 5C). We found that all types of currents were inhibited by D-AP5 but only gFICs and gSICs were inhibited by ifenprodil suggesting that they are mediated by GluN2B-containing extra-synaptic NMDA receptors (Figure 5C and 5D). We observed that TFLLR application did not cause any change in the frequency of mEPSC (Figure 5D), whereas TFLLR caused a significant increase in the frequency of both gFICs and gSICs in the Control condition (Figure 5D In acute slices of the control group, we observed that while both baseline and TFLLR-induced gFIC were blocked by astrocytic intracellular vesicle release inhibitor, Tetanus neurotoxin light chain (TeNTx), baseline and TFLLR-induced gSIC were blocked by TREK-1 blocker, spadin (Figure 5E). In GFAP::Opto-vTrap injected mice, we observed that the TFLLR-induced increase in the frequency of gFICs was completed prevented by 300 μW of continuous blue-light illumination, which fully recovered 15 minutes after light-off (Figure 5F and G), indicating that gFICs are mediated by a vesicular release mechanism. In contrast, the TFLLR-induced increase in frequency of gSICs was not affected by light illumination (Figure 5F and G), indicating that gSICs are mediated by non-vesicular,

channel-mediated release mechanism. Taken together, these results indicate that Opto-vTrap can be utilized as a fast and reversible optogenetic inhibition tool for vesicular gliotransmitter release.

Activation of Opto-vTrap reversibly inhibits contextual fear memory retrieval

As a final test, we investigated whether activation of Opto-vTrap can inhibit behavior, i.e., hippocampus-dependent contextual memory. The hippocampus has long been implicated in the spatial and contextual processing of fear memory (Arias et al., 2015; Fanselow and LeDoux, 1999; Kim and Fanselow, 1992). Hippocampal CA3-CA1 synaptic plasticity is modulated during memory acquisition, extinction, retrieval, and reconditioning of an associative learning in activity-dependent manner (Gruart et al., 2006). Since it has been reported that lesion of the hippocampal CA3 region causes impaired spatial memory retention in a rat model (Hunsaker et al., 2009; Steffenach et al., 2002), we examined whether inhibition of Schaffer collateral pathway by activation of Opto-vTrap impairs contextual memory retrieval. We injected CamKIIa::Opto-vTrap lentivirus into hippocampal CA3 regions uni-laterally and implanted optic cannula into CA1 region for light-illumination (Figure 6A). As a vector control without Opto-vTrap, we injected CMV::mCherry lentivirus. 3 weeks after the surgery, each Opto-vTrap-injected mouse was subjected to contextual fear conditioning on Day 1 (Figure 6A). On Day 2, each mouse was placed in the same context where the mouse acquired fear memory for three sessions of 3 min each with 1 hour interval between two sessions (Figure 6B). For activation of Opto-vTrap, we illuminated 1.0 mW of continuous blue-light during Trial 2 for 3 minutes on Day 2 (Figure 6B). As a control condition with no-light illumination, each mouse was subjected to additional contextual memory retrieval test on Day3 (Figure 6B). We observed that the freezing behavior was significantly decreased during a uni-lateral activation of Opto-vTrap in Trial 2, which was fully rescued one hour after the laser-off Trial 3 (Figure 6C and 6D). In contrast, the freezing behavior on Day 3 was not significantly changed during Trials 4 -6 in the absence of light-illumination (Figure 6B and 6C). The freezing behavior was not significantly changed during Trials 1-3 on Day2 in CMV::mCherry injected group (Figure 6D). These results indicate that inhibition of the

Schaffer-collateral pathway by activation of Opto-vTrap can effectively and reversibly impair fear memory retrieval with a full recovery within 1 hour. We also performed open field test and novel object recognition test without light illumination and there was no significant difference between control and Opto-vTrap expressing group. In addition, we observed that Opto-vTrap can efficiently and reversibly inhibit behavior in a continuous behavioral paradigm (Figure S7). Taken together, these results suggest that Opto-vTrap can be utilized in behaving animals to spatially, temporally, and cell-type-specifically silence brain circuit and behavior by light-illumination with a fast onset and fast recovery time.

Discussion

The newly developed Opto-vTrap is a highly effective optogenetic trap for light-induced reversible inhibition of vesicular release, synaptic transmission, gliotransmission and behavior. By bypassing the membrane potential change and directly targeting the vesicular exocytic machinery, we have been able to circumvent many confounding effects that are notoriously known for Arch and NpHR, such as hyperpolarization-induced rebound spikes and residual Ca^{2+} in presynaptic terminals. These unique advantages of Opto-vTrap, i.e., voltage-independence and Ca^{2+}-independence, implicate its broad applicability not only in neurons, but also in non-excitable cells such glial cells, endocrine cells, and any other secretory cells that do not express a host of voltage-gated ion channels to mediate action potentials or rebound spikes. Its broad applicability should also include possible uses in *in vitro* models of cell culture and organoid systems, *ex vivo* models of brain slices of various regions, *in vivo* animal models of behaving animals. These advantages place Opto-vTrap at the top of the list of choices for optogenetic probe for inhibition.

Opto-vTrap shows higher inhibition efficiency than other method for inhibition of synaptic transmission, such as Gi-DREADD system. It has been previously reported that locally expressing AAV-hM4Di in hippocampal CA3 shows about 30% block of fEPSP by bath perfusion of clozapine-

N-oxide, the agonist of hM4Di (Katzel et al., 2014). We observed about 45% block of eEPSC (Figure 4H) upon activation of Opto-vTrap. In contrast, we observed almost complete inhibition of TFLLR-induced increase in frequency of gFIC and a significant decrease in frequency of basal gFIC (Figure 5F). It appears that glial vesicular release was almost completely inhibited by activation of Opto-vTrap, while synaptic vesicular release was blocked by only a half. This discrepancy can be explained when we consider the bilateral projection from CA3 to CA1 in the hippocampus. Hippocampal CA1 inputs come from not only ipsilateral CA3-CA1 Shaffer collateral pathway, but also contralateral CA3 commissural pathway (Bliss et al., 1983). Moreover, there are some reports that both ipsilateral and contralateral projections equivalently contribute to synaptic plasticity in rodent model (Bliss *et al.*, 1983; Kohl et al., 2011; Shipton et al., 2014). Therefore, the partial block of evoked-EPSC is most likely due to the remaining synaptic release from the Opto-vTrap-non-expressing fibers, such as contralateral CA3 commissural projection, during electrical stimulation of Shaffer collateral pathway in *stratum radiatum* of the hippocampus. In contrast, the gFIC current, which showed almost complete inhibition by Opto-vTrap activation, occurs only in the local area where Opto-vTrap was expressed. In addition, Opto-vTrap virus transduction efficiency might slightly affect already high inhibition efficiency. Thus, we propose that the expression and activation of Opto-vTrap can inhibit vesicular release at high efficiency. We also performed contextual fear memory retrieval test to verify whether Opto-vTrap is applicable in behaving animal. We unilaterally targeted the same CA3-CA1 circuit, which had been tested by Opto-vTrap with high efficiency in acute brain slices. We observed about 25% block of memory retrieval upon Opto-vTrap activation (Figure 6C and D), which is a relatively lower value than other experimental results. It is well known that various circuits are involved in contextual memory retrieval process, such as both CA3-CA1, CA1-amygdala or CA1-mPFC (Jimenez et al., 2020; Liu et al., 2012; Orsini et al., 2011; Xu et al., 2016). Given the unilateral inhibition of CA3-CA1 circuit by Opto-vTrap and the possibility of other circuits involved during contextual memory retrieval, a 25% block of memory retrieval should be considered significant. Thus, we propose that Opto-vTrap can inhibit a specific circuit with high efficiency in behaving animal.

One of the most prominent advantages of Opto-vTrap is its fast recovery time. After an immediate clustering, Opto-vTrap took about 15 minutes to fully decluster (Figure 2D). The similar 15-minute recovery time was observed with the vesicular gliotransmission (Figure 5F and 5G). Finally, in the fear memory retrieval test we observed a complete recovery of impaired memory retrieval by activation of Opto-vTrap within one hour (Figure 6C). Although we could not test shorter intervals due to the nature of the behavioral test, it is possible that the recovery time of behavior could be shorter than one hour based on the *in vitro* results (Figure 2D and 5D). It will be interesting to test shorter recovery time with other behavioral tests that require a shorter interval between two consecutive sessions. Nevertheless, the observed one hour recovery time of Opto-vTrap is far superior than other optogenetic probes such as PA-BoNT and InSynC, which show a very long recovery time of about 24 hours (Lin *et al.,* 2013; Liu *et al.,* 2019). The critical difference is that an activation of Opto-vTrap does not induce any protein damage, which would take a long time for damaged proteins to be replenished by *de novo* protein synthesis. Indeed, we investigated whether inhibition of dopamine release from the terminals of SNpc neurons at dorsal striatum by Opto-vTrap causes real-time motor behavior deficit as a preliminary experiment (Figure S7). We observed a significant decrease in moving activities within 10 minutes of light stimulation and a recovery after light off (S7C and S7D), although the detailed mechanism of reduction in motion upon Opto-vTrap activation needs future investigations. Such a fast recovery time should provide a greater flexibility with the types of behavioral tests that can be adopted with Opto-vTrap.

Another important advantage of Opto-vTrap comes from the fact that its design is based on LARIAT, which utilizes CIBN and CRY2 interaction upon light-illumination. Recently, we have further developed various versions of LARIAT-derived optogenetic tools, such as IM-LARIAT and mRNA-LARIAT (Kim et al., 2020a; Nguyen et al., 2016), in which the basic principle of LARIAT has been applied to induce a rapid intracellular membrane aggregation and inhibition of translation of specific mRNA, respectively. Likewise, we have developed a new version of LARIAT-derived Opto-vTrap which inhibits vesicular exocytosis by clustering vesicles through VAMP2, which unspecifically targets various exocytic vesicles. Based on a similar concept, it should be possible to

use different target proteins such as vGluT, vGAT, and vMAT to specifically target a subtype of vesicles containing glutamate, GABA, and dopamine, respectively. We expect that not only synaptic transmitter or gliotransmitter release, but also dense core vesicle-containing small peptide release could be blocked by Opto-vTrap (Figure 3). We have also developed much-enhanced versions of CRY2 variants for CRY2:CRY2 homo dimerization such as CRY2clust and CRY2^{E281A}-A9 (Park et al., 2017) (Kim et al., 2020b). CRY2clust shows enhanced clustering property compare to currently used CRY2PHR (Park *et al.*, 2017), whereas CRY2^{E281A}-A9 shows ultra-high light-sensitivity to allow non-invasive light-stimulation without a need for insertion of fiber optic cables (Kim *et al.*, 2020b). Adopting these CRY2 variants to Opto-vTrap will be a natural course to take and should enhance the clustering property and light-sensitivity of the existing Opto-vTrap. These exciting possibilities await future investigations.

In summary, the basic concepts and molecular tools that we have developed in this study should be very useful for delineating circuit-level mechanisms of how various brain regions contribute to cognition and behavior. Furthermore, LARIAT-based Opto-vTrap promises futuristic development of new versatile and flexible optogenetic tools.

Acknowledgements

This work was supported by the Institute for Basic Science (IBS), Center for Cognition and Sociality (IBS-R001-D2). This paper is based on a research which has been conducted as part of the KAIST-funded Global Singularity Research Program for 2021. This work was supported by the National Research Foundation of Korea (NRF-2020R1A2C3014742).

Author Contributions

J.W., C.J.L., and W.D.H. designed the study, analyzed the data and wrote the manuscript. J.W and S.L performed and analyzed confocal imaging of Opvo-vTrap. J.W. performed and analyzed TIRF microscopy imaging. J.W., M.W.J., S.K., and Y.J. performed and analyzed membrane potential and eEPSC measurement. Y.P. performed and analyzed NMDAR-mediated spontaneous current

measurement. J.W. and A.K. performed and analyzed the fear conditioning behavior test. J.W. and S.P. performed and analyzed the animal motor activity inhibition test. J.W. and S.E.L. designed viral vector construct.

Competing Interests statement

The authors declare no competing financial interests.

STAR Methods

Lead contact

Further information and requests for resources and reagents should be directed to and will be fulfilled by the Lead Contact, C. Justin Lee (cjl@ibs.re.kr) or Won Do Heo (wondo@kaist.ac.kr).

Materials availability

Plasmids generated in this study will be deposited to Addgene.

Data and Code Availability

Raw data and analysis code are available without restriction from the Lead Contact.

EXPERIMENTAL MODEL AND SUBJECT DETAILS

Animals

For electrophysiology in brain acute slice, male C57BL/6J mice (6-10-week-old) were used. For behavioral test, male C57BL/6J (10-14-week-old) were used. All mice were maintained by trained facaulty of departmental animal facility, with 12:12-h light–dark cycle (lights on 8:00 A.M.) and free access to rodent chow and reverse osmotic water. All experimental procedures were conducted in accordance with the Institutional Animal Care and Use Committee (IACUC) of Korea Institute of Science and Technology (Seoul, Korea) and Institute of Basic Science (Deajeon, Korea).

Cell lines

For the *in vitro* imaging, COS-7 cells (#21651, Korean Cell Line Bank) and Neuroscreen-1 cells (NS-1, subclone of PC12 cells; Cellomics) were used. COS-7 cells were maintained in 90% Dulbecco's modified Eagle's medium (DMEM, #10-013-CV, Corning®) with 10% heat-inactivated fetal bovine serum (FBS, #10082147, Gibco™, Life technologies) at 37 °C and 10% CO_2. NS-1 cells

were provided by T. Meyer (Stanford University) and maintained in 80% Ham's F-12K (Kaighn's) Medium (#21127022, Gibco™, Life technologies) with 15% heat-inactivated horse serum (#26050088, Gibco™, Life technologies) and 5% heat-inactivated FBS (#10082147, Gibco™, Life technologies) at 37 °C and 5% CO_2. All cell lines were confirmed to be free from mycoplasma by using e-Myco Mycoplasma PCR detection kit (ver. 2.0, iNtRON).

Preparation of DNA construct

Mus musculus VAMP2 containing vector (VAMP2-BTX) was provided by J. Sanes (Harvard University). CRY2PHR-mCherry and CIBN-pmEGFP coding vectors were provided by C.L.Tucker (University of Colorado). For cloning the CIBN-mCherry-VAMP2 construct, sequence encoding CIBN (amino acid 1-170 of CIB1) and VAMP2 are PCR-amplified and restricted by NheI/AgeI and XhoI/EcoRI, respectively. The enzyme restricted CIBN and VAMP2 were inserted into corresponding sites of EGFP-C1 vector (Clontech). For cloning the PHR-mCitrine construct, we used a codon-optimized PHR (amino acids 1-498 of CRY2), which has been described in the previous paper (Lee *et al.*, 2014; Nguyen *et al.*, 2016). NheI/AgeI-restricted Codon-optimized PHR are inserted into corresponding sites of pmcitrine-C1 (Clontech). For cloning the PHR-iRFP682 construct, we replaced mCitrine with iRFP682 from iRFP682-N1 vector (Clontech) in PHR-mCitrine construct. For cloning the PHR-P2A-CIBN-mCherry-VAMP2, we amplified PHR and CIBN-mCherry-VAMP2, respectively, with a tagging P2A sequence. PCR-amplified and P2A sequence containing fragments were recombinant with NheI/XhoI restricted pECFP-C1 vector (Clontech) with In-Fusion® HD Cloning Kit (#639649, Clontech). For cloning pLenti-CamkIIa-PHR-P2A-CIBN-mCherry-VAMP2, we firstly cloning pAAV-CamIIa-PHR-P2A-CIBN-mCherry-VAMP2 by inserting AscI/NheI restricted PHR-P2A-CIBN-mCherry-VAMP2 into corresponding sites of pAAV-CaMKIIa-eArchT3.0-P2A-EGFP-WPRE-hGHpA (Clonetech). PCR-amplified CamKIIa-PHR-P2A-CIBN-mCherry-VAMP2 was recombinant with PacI/EcoRI restricted pLenti-CaMKIIa-ChETA-EYFP vector (Clontech) with In-Fusion® HD Cloning Kit (#639649, Clontech). For cloning AAV-CK(0.4)-PHR-P2A-CIBN-mCherry-VAMP2, PCR-amplified CK(0.4) from AAV-CK(0.4)GW (Stratagene) was enzymatic ligated with MluI/NheI restricted pAAV-pAAV-CamIIa-PHR-P2A-CIBN-mCherry-

VAMP2. For cloning pLenti-GFAP-PHR-P2A-CIBN-mCherry-VAMP2, PacI/BamHI restricted PCR-amplified GfaABC1D promoter was inserted into corresponding sites pLenti-CamKIIa-PHR-P2A-CIBN-mCherry-VAMP2. For cloning pLenti-DDC-PHR-P2A-CIBN-mCherry-VAMP2, MluI/NheI restricted PCR-amplified DDC promoter was inserted into corresponding sites pLenti-CamKIIa-PHR-P2A-CIBN-mCherry-VAMP2.

Transfection and live-cell imaging

For confocal live-cell imaging, COS-7 cells were transfected by electroporation (Neon™ Transfection System, Invitrogen) followed by the manufacturer's recommendations. In brief, 1×10^6 COS-7 cells were mixed with a total of 1 μg DNA and electroporated by 2 pulses of 1050 V for 30 msec. 5×10^4 of transfected cells were plated onto each μ-Plate 96 Well ibiTreat well (ibidi, 89626). After the transfection, we covered the plate with aluminum foil to prevent exposure to the light before the experiment. After 20-24 hours, we replace to fresh media and imaging. Live-cell confocal imaging was performed by using a Nikon A1R confocal microscope mounted onto a Nikon Eclipse Ti body and equipped with a CFI Plan Apochromat VC objectives (60×, numerical aperture (NA) 1.4, oil, Nikon Instruments). A Live-cell imaging chamber and incubation system were used for maintaining environmental conditions at 37 °C and 10% CO_2 (Live Cell Instruments). Images were acquired and processed by using (NIS-element AR, Nikon Instruments) and light stimulation was performed with a 488-nm laser with around 6.5 μW laser power. For image analysis, NIS-element (Nikon) and ImageJ software were used. Puncta signal was defined as 0.3-2.0 micron square size, circularity 0.0-1.0 in NIS-element (Nikon).

For TIRF imaging, 5×10^4 of NS-1 cells were plated on 8-well Lab-Tek II Chambered Coverglass (#155409, Thermo Scientific) and transfected by Lipofectamine LTX (Invitrogen) followed by manufacturer's recommendations. In brief, a dilute total of 0.2 μg DNA into 20 μl Opti-MEM™ I Reduced Serum Medium (#31985062, Gibco™, Life technologies) were mixed with Lipofectamine LTX reagent. And then, the DNA and reagent mixture was carefully added with fresh media into each well. After the transfection, we covered the plate with aluminum foil to prevent

exposure to the light before the experiment. After 20-24 hours, we replace to fresh media and imaging. TIRF imaging was performed at room temperature (25℃) by using a Nikon Ti-E TIRF microscope equipped with a CFI Apochromat TIRF 60× objective (Nikon Instruments). 488-nm laser (CVI-Melles Griot) was used to visualize neuropeptide Y-VENUS and light stimulation, simultaneously. To induce exocytosis, high-KCl containing Ringer's solution (70 mM KCl, 67 mM NaCl, 1 mM MgCl2, 2 mM CaCl2, 10 mM HEPES, and 2.8 mM glucose) was treated into imaging well.

Stereotaxic surgery and viral injection

All viruses were generated from the KIST Virus Facility (http://virus.kist.re.kr) or IBS Virus Facility (http://www.ibs.re.kr/virusfacility). For the viral injection for electrophysiology, mice were anesthetized with 300 mg/kg body weight of 2,2,2-tribromoethanol (#T48402, Sigma-Aldrich). Lentivirus of Lenti-CamKIIa::PHR-P2A-CIBN-mCherry-VAMP2 or AAV-DDC::PHR-P2A-CIBN-mCherry-VAMP was stereotactically injected into the hippocampal CA3 regions (for 6-7-week-old mice, -1.94 mm lambda from bregma, ± 2.28 mm lateral to the midline, -2.10 mm ventral from the brain surface) by using SP100IZ syringe pump (WPI). Lenti-GFAP::PHR-P2A-CIBN-mCherry-VAMP2 was stereotactically injected into the neocortex layer 2/3. For the behavior experiment with optic stimulation, mice were firstly anesthetized with 4% of isoflurane and oxygen mixture, and re-anesthetized with 20 mg/kg body weight of ketamine. A heating pad was used to maintain body temperature at 36 °C. Lentivirus of Lenti-CamKIIa::PHR-P2A-CIBN-mCherry was stereotactically injected into the hippocampal CA3 regions (for 8-10-week-old mice, -1.94 mm lambda from bregma, ± 2.3 mm lateral to the midline, -2.12 mm ventral from the brain surface) by using pressure (Picospritzer III, Parker Hannifin Corp.). Lentivirus of Lenti-DDC::PHR-P2A-CIBN-mCherry was stereotactically injected into the SNpc regions (for 7-9-week-old mice, -3.2 mm lambda from bregma, ± 1.7 mm lateral to the midline, -3 mm ventral from the brain surface) by using syringe pump (KD Scientific). The optic cannula (R-FOC-L100C-22NA, ceramic ferrule-Ø1.25mm/100um/0.22NA, RWD) was targeted to the hippocampal CA1 regions (-1.94 mm lambda from bregma, ± 1.3 mm

lateral to the midline, -1.20 mm ventral from the brain surface). After optic cannula implantation, dental cement was applied to cover the skull.

Immunohistochemistry of brain slice and super resolution imaging

For immunostaining, mice were anesthetized with intraperitoneal injection of 2% of 2, 2, 2-Tribromoethanol and perfused with 0.9% of normal saline, followed by ice-cold 4% paraformaldehyde (PFA). Extracted brains were postfixed in 4% of PFA at 4°C during 24 hrs followed by dehydrogenized in 30% sucrose containing PBS during 24 hrs. Brain slices were prepared as 30μm thickness by a cryostat and stored in storage solution at 4°C. Brain slices were washed in PBS and incubated in blocking solution (0.3% Triton X-100, 2% donkey serum, 2% goat serum, in 0.1M of PBS) for 1 hr. Brain slices were immunostained in primary antibodies (ab167453, Anti-mCherry antibody, abcam; NB120-13249, Novus Biologicals, anti-Bassoon antibody (SAP7F407); ab133856, Anti-SYT1 antibody, abcam) containing blocking solution on shaker at 4°C during 18 hrs. After primary immunostaining, slices were washed in PBS at room and second immunostained in corresponding fluorescence-conjugating secondary antibodies containing blocking solution during 1 hr and then washed in PBS. Brain sections were mounted with fluorescent mounting media (S3023, Dako). A series of fluorescent images were obtained with an Eylra 7 Zeiss super resolution microscope. 3D imaging rendering and analysis were performed by IMARIS software.

Slice patch-clamp recording

For the eEPSC recording, mice were anesthetized with isoflurane and decapitated. The 300 μm coronal slices of hippocampus were prepared in ice-cooling sucrose-based cutting solution (sucrose, 234 mM; KCl, 2.5 mM; MgSO4, 10 mM; NaH2PO4, 1.25 mM; NaHCO3, 24 mM; CaCl2-2H2O, 0.5 mM; and glucose, 11 mM) on D.S.K Linear Slicer pro7 (Dosaka EM Co., Ltd). For evoked-EPSC recording, slices were recovered for at least 1 hour before recording in oxygenated aCSF (NaCl, 126 mM; NaHCO3, 24 mM; KCl, 2.5 mM; NaH2PO4, 1mM; MgCl2, 2 mM; and glucose, 10 mM). For miniature EPSC recording, 1 μM of TTX was added to oxygeneated aCSF. For evoked EPSC and miniature EPSC recording, current was recorded under oxygenated aCSF solution by whole-cell

voltage-clamp. Recording electrode (5-8 MΩ) was fabricated standard-wall borosilicate glass (GC150F-10, Warner Instrument Corp., USA) and filled with an $CeMeSO_4$-based internal solution ($CeMeSO_4$, 132 mM; NaCl, 8 mM; HEPES, 10 mM; EGTA, 0.25 mM; Mg-ATP, 2 mM; and Na_2-GTP, 0.5 mM; QX-314, 1 mM; with pH adjusted to 7.3 and osmolality adjusted to 295 mOsmol/kg). Synaptic activity was evoked by paired-stimulus of Schaffer collateral pathway (0.1 ms, 50 mA~500 mA, 100 msec interval) using a tungsten bipolar electrode holding at -60 mV.

For the membrane potential recording, mice were anesthetized with isoflurane and decapitated. The 300 μm coronal slices of hippocampus were prepared in ice-cooling NMDG-based cutting solution (NMDG, 93 mM; KCl, 2.5 mM; NaH2PO4, 1.2 mM; NaHCO3, 30 mM; HEPES, 20 mM; Glucose, 25 mM; Sodium ascorbate, 5 mM; Thourea, 2 mM; Sodium pyruvate, 3 mM; $MgCl_2$, 10 mM; $CaCl_2$, 0.5 mM, pH adjusted to 7.3 with HCl, 310 mOsm). Slices were recovered 15 minutes at 32℃ in the same solution. For current injection, current was injected from -100 pA, -20 pA increment upto +100 pA. Membrane potential was recorded under oxygenated aCSF solution. Recording electrodes (5-8 MΩ) was fabricated standard-wall borosilicate glass (GC150F-10, Warner Instrument Corp., USA) and filled with an K-gluconate-based internal solution (120 mM potassium gluconate; 10 mM KCl; 1 mM MgCl2; 0.5 mM EGTA; 40 mM HEPES; with pH-adjusting to 7.2 and osmolality adjusting to 300 mOsmol/kg). All recordings are performed at room temperature (25℃).

Animal behavior test

For the contextual fear memory retrieval test, 11-13-weeks-old male mice were individually placed in fear conditioning chambers (Coulbourn Instruments). After a 2.5 min habituation period, a 1 second foot shock (1 mA) was delivered every 1 minute for 2.5 min (total, 3 times shocks) on Day 1. To assess fear contextual memory, the mice were placed back into the same chamber 24 hr after acquisition (Day 2). During all trials of contextual memory retrieval test, optic fiber was connected to optic cannula which was implanted into hippocampal CA1 regions. On Day 2, contextual fear retrieval test was carried out 3 times (trial 1-3) in 1 hour interval. 1.0 mW of 488 nm laser was turned on only in trial 2. On Day 3, contextual fear retrieval test was carried out 3 times (trial 4-6) without laser. The

behavior of the mice was recorded with the Freezeframe software (Coulbourn Instruments) and analyzed with Freezeview software (Coulbourn Instruments). For open field test, 10-12-weeks-old male mice were individually placed in white acryl container (40 cm × 40 cm × 40 cm) and allowed to freely move to chamber for 10 minutes for habituation. Animals were allowed to freely explore the apparatus for 10 minutes. The open field was divided into a central zone (12 cm × 12 cm) and a peripheral zone and traveled distance and velocity were analyzed using Ethovision XT software (Noldus). For novel place recognition test, 10-12-weeks-old male mice were individually placed in white acryl container (40 cm × 40 cm × 40 cm) with two identical objects positioned in the first and the second quadrant of the cage (Figure S6) and allowed to freely explore to the objects for 10 minutes (familiarization session). Then, mice were transferred to their home cage for 1 hour. After 1 hour, mice were re-placed to acryl container with two identical objects positioned in the first and the fourth quadrant of the cage (Figure S6 D) and allowed to freely explore the objects for 10 minutes (test session). The exploration behavior of each mice was monitored by a video camera and analyzed manually by an experimenter.

QUANTIFICATION AND STATISTICAL ANALYSIS

All analyses were done blindly. The number of experimental samples, mean and SEM values are listed in Figure legends. The numbers and individual dots refer to the number of cells unless otherwise clarified in figure legends. For data presentation and statistical analysis, Graphpad Prism (GraphPad Software) was used. For analyze for electrophysiology, Clampfit (Molecular Devices) and Mini analysis (Synaptosoft) were used. For behavioral analysis, Ethovision XT (Noldus) and Freezeview(Coulbourn Instruments) were used. For image analysis, NIS-element (Nikon) and Imagej software were used. Statistical significance was set at *$p < 0.05$, **$p < 0.01$, ***$p < 0.001$, ****$p < 0.0001$. Data are presented as mean ± SEM.

Reference

Amaral, D.G., and Witter, M.P. (1989). The three-dimensional organization of the hippocampal formation: a review of anatomical data. Neuroscience *31*, 571-591. 10.1016/0306-4522(89)90424-7.

Arias, N., Mendez, M., and Arias, J.L. (2015). The importance of the context in the hippocampus and brain related areas throughout the performance of a fear conditioning task. Hippocampus *25*, 1242-1249. 10.1002/hipo.22430.

Armbruster, B.N., Li, X., Pausch, M.H., Herlitze, S., and Roth, B.L. (2007). Evolving the lock to fit the key to create a family of G protein-coupled receptors potently activated by an inert ligand. Proc Natl Acad Sci U S A *104*, 5163-5168. 10.1073/pnas.0700293104.

Becherer, U., Pasche, M., Nofal, S., Hof, D., Matti, U., and Rettig, J. (2007). Quantifying exocytosis by combination of membrane capacitance measurements and total internal reflection fluorescence microscopy in chromaffin cells. PLoS One *2*, e505. 10.1371/journal.pone.0000505.

Bliss, T.V., Lancaster, B., and Wheal, H.V. (1983). Long-term potentiation in commissural and Schaffer projections to hippocampal CA1 cells: an in vivo study in the rat. J Physiol *341*, 617-626. 10.1113/jphysiol.1983.sp014828.

Boyden, E.S., Zhang, F., Bamberg, E., Nagel, G., and Deisseroth, K. (2005). Millisecond-timescale, genetically targeted optical control of neural activity. Nat Neurosci *8*, 1263-1268. 10.1038/nn1525.

Bugaj, L.J., Choksi, A.T., Mesuda, C.K., Kane, R.S., and Schaffer, D.V. (2013). Optogenetic protein clustering and signaling activation in mammalian cells. Nat Methods *10*, 249-252. 10.1038/nmeth.2360.

Chow, B.Y., Han, X., Dobry, A.S., Qian, X., Chuong, A.S., Li, M., Henninger, M.A., Belfort, G.M., Lin, Y., Monahan, P.E., and Boyden, E.S. (2010). High-performance genetically targetable optical neural silencing by light-driven proton pumps. Nature *463*, 98-102. 10.1038/nature08652.

Deak, F., Shin, O.H., Kavalali, E.T., and Sudhof, T.C. (2006). Structural determinants of synaptobrevin 2 function in synaptic vesicle fusion. J Neurosci *26*, 6668-6676. 10.1523/JNEUROSCI.5272-05.2006.

Dittgen, T., Nimmerjahn, A., Komai, S., Licznerski, P., Waters, J., Margrie, T.W., Helmchen, F., Denk, W., Brecht, M., and Osten, P. (2004). Lentivirus-based genetic manipulations of cortical neurons and their optical and electrophysiological monitoring in vivo. Proc Natl Acad Sci U S A *101*, 18206-18211. 10.1073/pnas.0407976101.

Dobrunz, L.E., and Stevens, C.F. (1997). Heterogeneity of release probability, facilitation, and depletion at central synapses. Neuron *18*, 995-1008. 10.1016/s0896-6273(00)80338-4.

Fanselow, M.S., and LeDoux, J.E. (1999). Why we think plasticity underlying Pavlovian fear conditioning occurs in the basolateral amygdala. Neuron *23*, 229-232. 10.1016/s0896-6273(00)80775-8.

Gruart, A., Munoz, M.D., and Delgado-Garcia, J.M. (2006). Involvement of the CA3-CA1 synapse in the acquisition of associative learning in behaving mice. J Neurosci *26*, 1077-1087. 10.1523/JNEUROSCI.2834-05.2006.

Harada, K., Kamiya, T., and Tsuboi, T. (2015). Gliotransmitter Release from Astrocytes: Functional, Developmental, and Pathological Implications in the Brain. Front Neurosci *9*, 499. 10.3389/fnins.2015.00499.

Hastoy, B., Scotti, P.A., Milochau, A., Fezoua-Boubegtiten, Z., Rodas, J., Megret, R., Desbat, B., Laguerre, M., Castano, S., Perrais, D., et al. (2017). A Central Small Amino Acid in the VAMP2 Transmembrane Domain Regulates the Fusion Pore in Exocytosis. Sci Rep *7*, 2835. 10.1038/s41598-017-03013-3.

Hayashi, T., McMahon, H., Yamasaki, S., Binz, T., Hata, Y., Sudhof, T.C., and Niemann, H. (1994). Synaptic vesicle membrane fusion complex: action of clostridial neurotoxins on assembly. EMBO J *13*, 5051-5061.

Hollenberg, M.D., Saifeddine, M., al-Ani, B., and Kawabata, A. (1997). Proteinase-activated receptors: structural requirements for activity, receptor cross-reactivity, and receptor selectivity of receptor-activating peptides. Can J Physiol Pharmacol *75*, 832-841.

Hunsaker, M.R., Tran, G.T., and Kesner, R.P. (2009). A behavioral analysis of the role of CA3 and CA1 subcortical efferents during classical fear conditioning. Behav Neurosci *123*, 624-630. 10.1037/a0015455.
Jimenez, J.C., Berry, J.E., Lim, S.C., Ong, S.K., Kheirbek, M.A., and Hen, R. (2020). Contextual fear memory retrieval by correlated ensembles of ventral CA1 neurons. Nat Commun *11*, 3492. 10.1038/s41467-020-17270-w.
Karpova, A.Y., Tervo, D.G., Gray, N.W., and Svoboda, K. (2005). Rapid and reversible chemical inactivation of synaptic transmission in genetically targeted neurons. Neuron *48*, 727-735. 10.1016/j.neuron.2005.11.015.
Katzel, D., Nicholson, E., Schorge, S., Walker, M.C., and Kullmann, D.M. (2014). Chemical-genetic attenuation of focal neocortical seizures. Nat Commun *5*, 3847. 10.1038/ncomms4847.
Kennedy, M.J., Hughes, R.M., Peteya, L.A., Schwartz, J.W., Ehlers, M.D., and Tucker, C.L. (2010). Rapid blue-light-mediated induction of protein interactions in living cells. Nat Methods *7*, 973-975. 10.1038/nmeth.1524.
Kim, J.J., and Fanselow, M.S. (1992). Modality-specific retrograde amnesia of fear. Science *256*, 675-677. 10.1126/science.1585183.
Kim, N.Y., Lee, S., Yu, J., Kim, N., Won, S.S., Park, H., and Heo, W.D. (2020a). Optogenetic control of mRNA localization and translation in live cells. Nat Cell Biol *22*, 341-352. 10.1038/s41556-020-0468-1.
Kim, S., Kyung, T., Chung, J.H., Kim, N., Keum, S., Lee, J., Park, H., Kim, H.M., Lee, S., Shin, H.S., and Do Heo, W. (2020b). Non-invasive optical control of endogenous Ca(2+) channels in awake mice. Nat Commun *11*, 210. 10.1038/s41467-019-14005-4.
Kohl, M.M., Shipton, O.A., Deacon, R.M., Rawlins, J.N., Deisseroth, K., and Paulsen, O. (2011). Hemisphere-specific optogenetic stimulation reveals left-right asymmetry of hippocampal plasticity. Nat Neurosci *14*, 1413-1415. 10.1038/nn.2915.
Lee, S., Park, H., Kyung, T., Kim, N.Y., Kim, S., Kim, J., and Heo, W.D. (2014). Reversible protein inactivation by optogenetic trapping in cells. Nat Methods *11*, 633-636. 10.1038/nmeth.2940.
Lee, Y., Messing, A., Su, M., and Brenner, M. (2008). GFAP promoter elements required for region-specific and astrocyte-specific expression. Glia *56*, 481-493. 10.1002/glia.20622.
Lin, J.Y., Lin, M.Z., Steinbach, P., and Tsien, R.Y. (2009). Characterization of engineered channelrhodopsin variants with improved properties and kinetics. Biophys J *96*, 1803-1814. 10.1016/j.bpj.2008.11.034.
Lin, J.Y., Sann, S.B., Zhou, K., Nabavi, S., Proulx, C.D., Malinow, R., Jin, Y., and Tsien, R.Y. (2013). Optogenetic inhibition of synaptic release with chromophore-assisted light inactivation (CALI). Neuron *79*, 241-253. 10.1016/j.neuron.2013.05.022.
Liu, Q., Sinnen, B.L., Boxer, E.E., Schneider, M.W., Grybko, M.J., Buchta, W.C., Gibson, E.S., Wysoczynski, C.L., Ford, C.P., Gottschalk, A., et al. (2019). A Photoactivatable Botulinum Neurotoxin for Inducible Control of Neurotransmission. Neuron *101*, 863-875 e866. 10.1016/j.neuron.2019.01.002.
Liu, X., Ramirez, S., Pang, P.T., Puryear, C.B., Govindarajan, A., Deisseroth, K., and Tonegawa, S. (2012). Optogenetic stimulation of a hippocampal engram activates fear memory recall. Nature *484*, 381-385. 10.1038/nature11028.
Mahn, M., Prigge, M., Ron, S., Levy, R., and Yizhar, O. (2016). Biophysical constraints of optogenetic inhibition at presynaptic terminals. Nat Neurosci *19*, 554-556. 10.1038/nn.4266.
Mattingly, M., Weineck, K., Costa, J., and Cooper, R.L. (2018). Hyperpolarization by activation of halorhodopsin results in enhanced synaptic transmission: Neuromuscular junction and CNS circuit. PLoS One *13*, e0200107. 10.1371/journal.pone.0200107.
Nagel, G., Szellas, T., Huhn, W., Kateriya, S., Adeishvili, N., Berthold, P., Ollig, D., Hegemann, P., and Bamberg, E. (2003). Channelrhodopsin-2, a directly light-gated cation-selective membrane channel. Proc Natl Acad Sci U S A *100*, 13940-13945. 10.1073/pnas.1936192100.
Nguyen, M.K., Kim, C.Y., Kim, J.M., Park, B.O., Lee, S., Park, H., and Heo, W.D. (2016). Optogenetic oligomerization of Rab GTPases regulates intracellular membrane trafficking. Nat Chem Biol *12*, 431-436. 10.1038/nchembio.2064.

Orsini, C.A., Kim, J.H., Knapska, E., and Maren, S. (2011). Hippocampal and prefrontal projections to the basal amygdala mediate contextual regulation of fear after extinction. J Neurosci *31*, 17269-17277. 10.1523/JNEUROSCI.4095-11.2011.
Park, H., Kim, N.Y., Lee, S., Kim, N., Kim, J., and Heo, W.D. (2017). Optogenetic protein clustering through fluorescent protein tagging and extension of CRY2. Nat Commun *8*, 30. 10.1038/s41467-017-00060-2.
Parpura, V., and Zorec, R. (2010). Gliotransmission: Exocytotic release from astrocytes. Brain Res Rev *63*, 83-92. 10.1016/j.brainresrev.2009.11.008.
Raimondo, J.V., Kay, L., Ellender, T.J., and Akerman, C.J. (2012). Optogenetic silencing strategies differ in their effects on inhibitory synaptic transmission. Nat Neurosci *15*, 1102-1104. 10.1038/nn.3143.
Rizo, J., and Xu, J. (2015). The Synaptic Vesicle Release Machinery. Annu Rev Biophys *44*, 339-367. 10.1146/annurev-biophys-060414-034057.
Rosenfeldt, G., Viana, R.M., Mootz, H.D., von Arnim, A.G., and Batschauer, A. (2008). Chemically induced and light-independent cryptochrome photoreceptor activation. Mol Plant *1*, 4-14. 10.1093/mp/ssm002.
Saloman, J.L., Scheff, N.N., Snyder, L.M., Ross, S.E., Davis, B.M., and Gold, M.S. (2016). Gi-DREADD Expression in Peripheral Nerves Produces Ligand-Dependent Analgesia, as well as Ligand-Independent Functional Changes in Sensory Neurons. J Neurosci *36*, 10769-10781. 10.1523/JNEUROSCI.3480-15.2016.
Schoch, S., Deak, F., Konigstorfer, A., Mozhayeva, M., Sara, Y., Sudhof, T.C., and Kavalali, E.T. (2001). SNARE function analyzed in synaptobrevin/VAMP knockout mice. Science *294*, 1117-1122. 10.1126/science.1064335.
Schoenenberger, P., Scharer, Y.P., and Oertner, T.G. (2011). Channelrhodopsin as a tool to investigate synaptic transmission and plasticity. Exp Physiol *96*, 34-39. 10.1113/expphysiol.2009.051219.
Shipton, O.A., El-Gaby, M., Apergis-Schoute, J., Deisseroth, K., Bannerman, D.M., Paulsen, O., and Kohl, M.M. (2014). Left-right dissociation of hippocampal memory processes in mice. Proc Natl Acad Sci U S A *111*, 15238-15243. 10.1073/pnas.1405648111.
Sollner, T., Bennett, M.K., Whiteheart, S.W., Scheller, R.H., and Rothman, J.E. (1993). A protein assembly-disassembly pathway in vitro that may correspond to sequential steps of synaptic vesicle docking, activation, and fusion. Cell *75*, 409-418. 10.1016/0092-8674(93)90376-2.
Steffenach, H.A., Sloviter, R.S., Moser, E.I., and Moser, M.B. (2002). Impaired retention of spatial memory after transection of longitudinally oriented axons of hippocampal CA3 pyramidal cells. Proc Natl Acad Sci U S A *99*, 3194-3198. 10.1073/pnas.042700999.
Sudhof, T.C. (2004). The synaptic vesicle cycle. Annu Rev Neurosci *27*, 509-547. 10.1146/annurev.neuro.26.041002.131412.
Sudhof, T.C. (2012). Calcium control of neurotransmitter release. Cold Spring Harb Perspect Biol *4*, a011353. 10.1101/cshperspect.a011353.
Weiss, N., Zamponi, G.W., and De Waard, M. (2012). How do T-type calcium channels control low-threshold exocytosis? Commun Integr Biol *5*, 377-380. 10.4161/cib.19997.
Wiegert, J.S., Mahn, M., Prigge, M., Printz, Y., and Yizhar, O. (2017). Silencing Neurons: Tools, Applications, and Experimental Constraints. Neuron *95*, 504-529. 10.1016/j.neuron.2017.06.050.
Woo, D.H., Han, K.S., Shim, J.W., Yoon, B.E., Kim, E., Bae, J.Y., Oh, S.J., Hwang, E.M., Marmorstein, A.D., Bae, Y.C., et al. (2012). TREK-1 and Best1 channels mediate fast and slow glutamate release in astrocytes upon GPCR activation. Cell *151*, 25-40. 10.1016/j.cell.2012.09.005.
Xu, C., Krabbe, S., Grundemann, J., Botta, P., Fadok, J.P., Osakada, F., Saur, D., Grewe, B.F., Schnitzer, M.J., Callaway, E.M., and Luthi, A. (2016). Distinct Hippocampal Pathways Mediate Dissociable Roles of Context in Memory Retrieval. Cell *167*, 961-972 e916. 10.1016/j.cell.2016.09.051.
Zhang, F., Wang, L.P., Brauner, M., Liewald, J.F., Kay, K., Watzke, N., Wood, P.G., Bamberg, E., Nagel, G., Gottschalk, A., and Deisseroth, K. (2007). Multimodal fast optical interrogation of neural circuitry. Nature *446*, 633-639. 10.1038/nature05744.

Zhou, Q., Zhou, P., Wang, A.L., Wu, D., Zhao, M., Sudhof, T.C., and Brunger, A.T. (2017). The primed SNARE-complexin-synaptotagmin complex for neuronal exocytosis. Nature *548*, 420-425. 10.1038/nature23484.

Figure Legends

Figure 1: Design and principle of Opto-vTrap

(A) Map of LARIAT components and Opto-vTrap construct. (**B**) Experimental scheme of working principle of Opto-vTrap. A blue light (488nm) illumination triggers heteromeric dimerization of CRY2:CIBN-VAMP and homomeric oligomerization of CRY2:CRY2, and induces vesicle clusterization. Thus, CIBN-VAMP2 targeting vesicles are reversibly clusterized upon blue light illumination.

Figure 2: Characterization of Opto-vTrap in COS-7 cells

(A) Experimental timeline and scheme of the live-cell imaging of Opto-vTrap. A blue laser was turned on (Light On) for 15 minutes. A 561 nm laser was used for CIBN-VAMP2 detection. A 0.2 Hz of 20% duty cycle of 488 nm laser was used for Opto-vTrap activation and CRY2 detection. (**B)** Confocal images of Opto-vTrap (CIBN-mCherry-VAMP2 and CRY2-mCitrine) expressing COS-7 cell. The yellow arrow indicates the position of the kymograph depiction in Figure 2C. (**C)** The Kymograph of CIBN-VAMP2 through the yellow arrow drawn in Figure 2B. Magenta arrows indicate the position of intensity profile depiction in Figure 2D. The timing of 488 nm laser is represented as a blue line. (**D)** The intensity profile of CIBN-VAMP2 through the magenta arrows from the kymograph in Figure 2C. (**E)** Representative quantification graph of the number of vesicle puncta in Figure 2B. The blue box indicates a 488 nm laser illumination for Opto-vTrap activation. **(F)** Individuals (grey) and averaged (black) quantification graph of the number of vesicle puncta. **(G)** Percent of CIBN-VAMP2 fluorescent puncta during Before, Light On, and 15 minutes after light off (After) (Before, averaged number of puncta in 0-5 min; Light On, maximum value during light On; After, averaged number of puncta at 25-30min, respectively). (n=10, data are presented as the mean ± s.e.m, ****$p<0.0001$, One-way ANOVA test). **(H)** Pearson's correlation coefficient (blue line) between CIBN-VAMP2-mCherry and CRY2-mCitrine after blue laser on (n=10, data are presented as the mean ± s.e.m) and non-linear fitting curve (black, one-phase association). **(I)** Representative

confocal images of Opto-vTrap (CIBN-mCherry-VAMP2 and CRY2-iFRP) expressing COS-7 cell. **(J)** Pearson's correlation coefficient (black line) between CIBN-VAMP2-mCherry and CRY2-iRFP682. The blue box indicates a 488 nm laser illumination (n=8, data are presented as the mean ± s.e.m).

Figure 3: Optogenetic inhibition of vesicular exocytosis by Opto-vTtrap in Neuroscreen-1 cells. **(A)** Experimental scheme of the vesicle exocytosis imaging under TIRF microscopy. In control, CIBN-VAMP2 and NPY-VENUS were expressed. In Opto-vTrap, CIBN-VAMP2, CRY2, and NPY-VENUS were expressed. NPY-VENUS was used as vesicle contents. Exocytosis events were triggered by high-KCl Ringer's solution. **(B)** Experimental timeline of the vesicle exocytosis imaging under TIRF microscopy. A 5 Hz of 40% duty cycle of 488 nm laser was used for NPY-VENUS detection and Opto-vTrap activation. **(C)** Representative TIRF microscopy images of Control and Opto-vTrap expressing Neuroscreen-1 cells. Green signals represent NPY-VENUS. **(D)** Representative images of Control and Opto-vTrap expressing Neuroscreen-1 cells 10 seconds after treatment of high-KCl Ringer's solution. Each circle indicates the NPY-VENUS containing vesicles and analyzed in Figure 3E. **(E)** Representative traces of NPY-VENUS in Control and Opto-vTrap expressing Neuroscreen-1 cell from Figure 2B-D. **(F)** Summary graph of percent of peak amplitude of NPY-VENUS puncta in control and Opto-vTrap expressing Neuroscreen-1 cell after high-KCl solution treatment (n=11, respectively, data are presented as the mean ± s.e.m ****P<0.0001, Mann-Whitney test).

Figure 4: Activation of Opto-vTrap inhibits evoked EPSC in Schaffer-collateral synapses **(A)** Map of Lentiviral CamKIIα::Opto-vTrap construct and injection strategy for Opto-vTrap expression. **(B)** Representative membrane potential trace in response to current injection in Opto-vTrap expressing cell. **(C)** Representative membrane potential trace in Opto-vTrap expressing cell. Blue line indicates blue light illumination. **(D)** Summary graph of membrane potential from Before and Light On conditions (n=5, Wilcoxon test). **(E)** Experimental scheme of eEPSC recording with

765 blue light illumination and representative traces of eEPSC in Control and Opto-vTrap injected brain
766 acute slices during Before, Light On, and After conditions, respectively (Scale bar: 20 ms, 100 pA.
767 P1: first-peak amplitude, P2: second-peak amplitude). **(F)** Summary bar graph of 1st amplitude during
768 paired-pulse stimulation in Control (left) and Opto-vTrap condition (right) (n=6, Control; n=9, Opto-
769 vTrap). **(G)** Percent of 1st amplitude during paired-pulse stimulation in Control (left) and Opto-vTrap
770 groups (right). Blue box indicates blue light illumination (0 to 15 min) (n=6, Control; n=9, Opto-
771 vTrap) **(H)** Summary bar graph of percent of 1st amplitude during Before, Light On and After
772 conditions in Control and opto-vTrap groups (n=7, Control; n=12, Opto-vTrap; ****P<0.0001, *p <
773 0.05, mixed-effects analysis). **(I)** Percent of 2nd amplitude during paired-pulse stimulation in Control
774 (left) and Opto-vTrap mice (right). Blue box indicates blue light illumination (0 to 15 min) (n=7,
775 Control; n=12, Opto-vTrap). **(J)** Summary bar graph of percent of 2nd amplitude during Before and
776 Light On, After conditions in Control and Opto-vTrap group (n=7, Control; n=12, Opto-vTrap; *p <
777 0.05, mixed-effects analysis). **(I)** Paired-pulse ratio during paired-pulse stimulation in Control (left)
778 and Opto-vTrap groups (right) (n=7, Control; n=12, Opto-vTrap). **(K)** Summary bar graph of paired-
779 pulse ratio during Before, Light On and After conditions in Control and Opto-vTrap (n=7, Control;
780 n=12, Opto-vTrap; mixed-effects analysis). Data are presented as the mean ± s.e.m.
781
782 **Figure 5: Activation of Opto-vTrap inhibits neocortical astrocytic vesicular gliotransmitter**
783 **release**
784 **(A)** Map of Lentiviral GFAP::Opto-vTrap construct and experimental strategy of astrocytic
785 exocytosis-mediated fast inward NMDAR-mediated current measurement. **(B)** Representative whole-
786 cell currents recording in the baseline, TFLLR application with blue light off, and TFLLR application
787 with Light On. **(C)** Kinetics of transient NMDAR-mediated currents in the neurons of GFAP::Opto-
788 vTrap condition. **(D)** Pooled data on the frequency of before (baseline) and after stimulation of
789 astrocytes with TFLLR in the Control (n=14, control; n=6, TFLLR+D-AP5; n=7, TFLLR+ifenprodil;
790 *p < 0.05, paired-t-test). **(E)** Pooled data of the frequency of gFIC and gSIC recorded after the
791 intracellular perfusion of astrocyte with Tetanus neurotoxin light chain (TeNTx, 3nM, 15 min prior to

recordings) or bath application of spadin (TREK-1 blocker, 200nM) (n=6, baseline; n=5, TFLLR; **p < 0.01, non-paired t-test). **(F)** Representative time course of the average amplitude and frequency of glia-induced fast (gFICs) and slow (gSICs) currents recorded in the neocortical neurons of Control (left) and Opto-vTrap (right) mice. The blue box indicates the timing of blue light illumination (5 to 20 min) (n=4, Control; n=4, Opto-vTrap, #p < 0.05, paired t-test). **(G)** Pooled data on the frequency of gFIC and gSIC during light off, light on, and light-off (n=4, baseline; n=4, TFLLR; *p < 0.05, non-paired-t-test). Data are presented as the mean ± s.e.m.

Figure 6: Activation of Opto-vTrap reversibly inhibits contextual fear memory retrieval

(A) Experimental strategy of Schaffer collateral pathway mediated memory retrieval (fear conditioning test) in opto-vTrap injected mice. **(B)** Experimental scheme of memory retrieval test. During contextual retrieval test in trial 1-6, blue laser was on in trial 2 only. **(C)** Percent of freezing of each Opto-vTrap mice during trials 1-3 and 4-6. The blue box indicates the timing of 488 nm laser exposure (trial 2 only) (n=6). **(D)** Normalized freezing behavior from Figure 6C. Percent freezing of trial 1-3 are normalized to trial 1, trial 4-6 are normalized to trial 4. (n=10, Control; n=6, Opto-vTrap; ****p<0.0001, in Opto-vTrap trial 2 vs. Opto-vTrap trial 5 and ***p<0.001 in Opto-vTrap trial 2 vs. Control trial 2, 2-way ANOVA; ####p<0.0001, RM one-way ANOVA in Opto-vTrap trial 1 vs. trial 2). Data are presented as the mean ± s.e.m.

Figure 1: Design and principle of Opto-vTrap

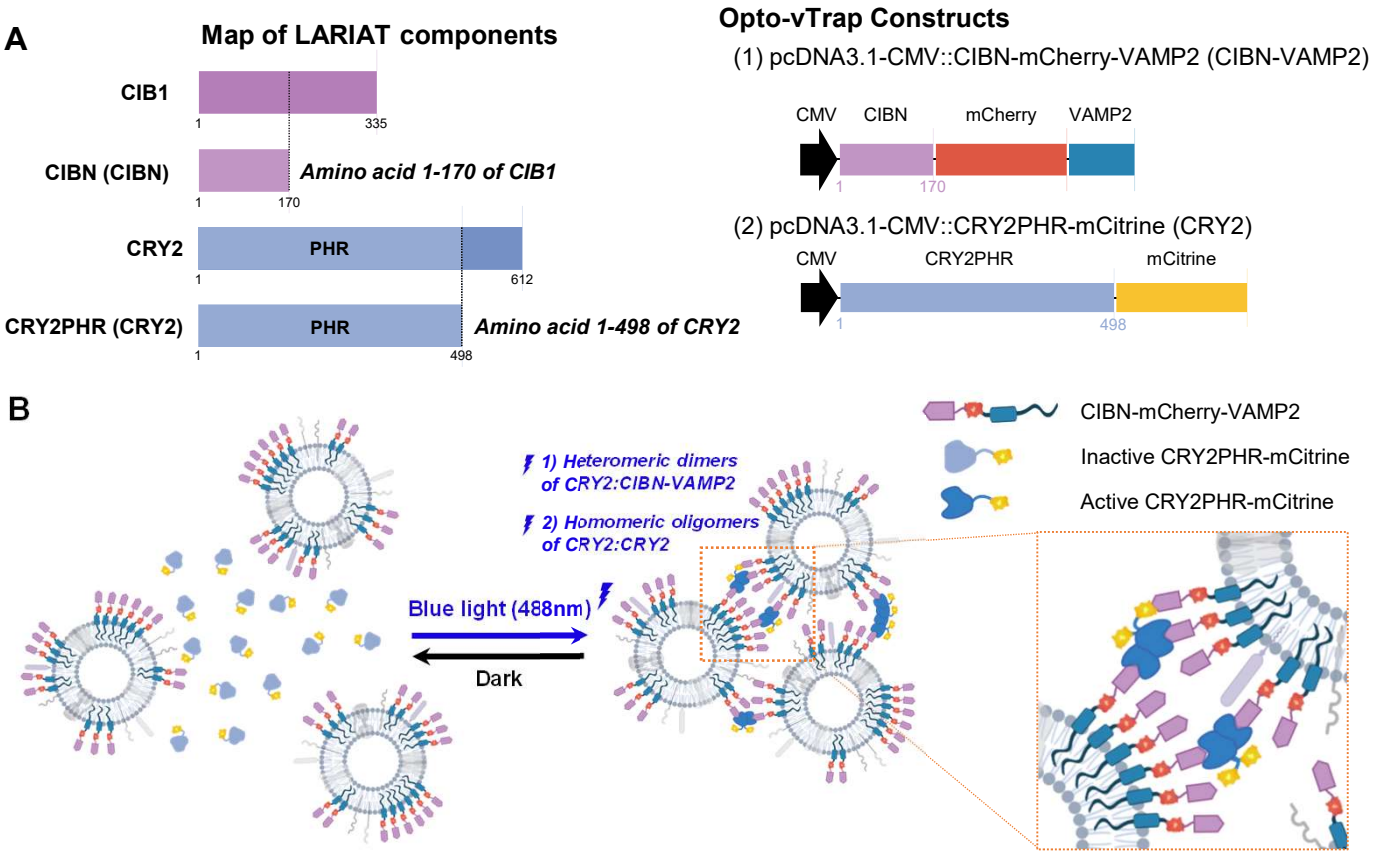

Figure 2: Characterization of Opto-vTrap in COS-7 cells

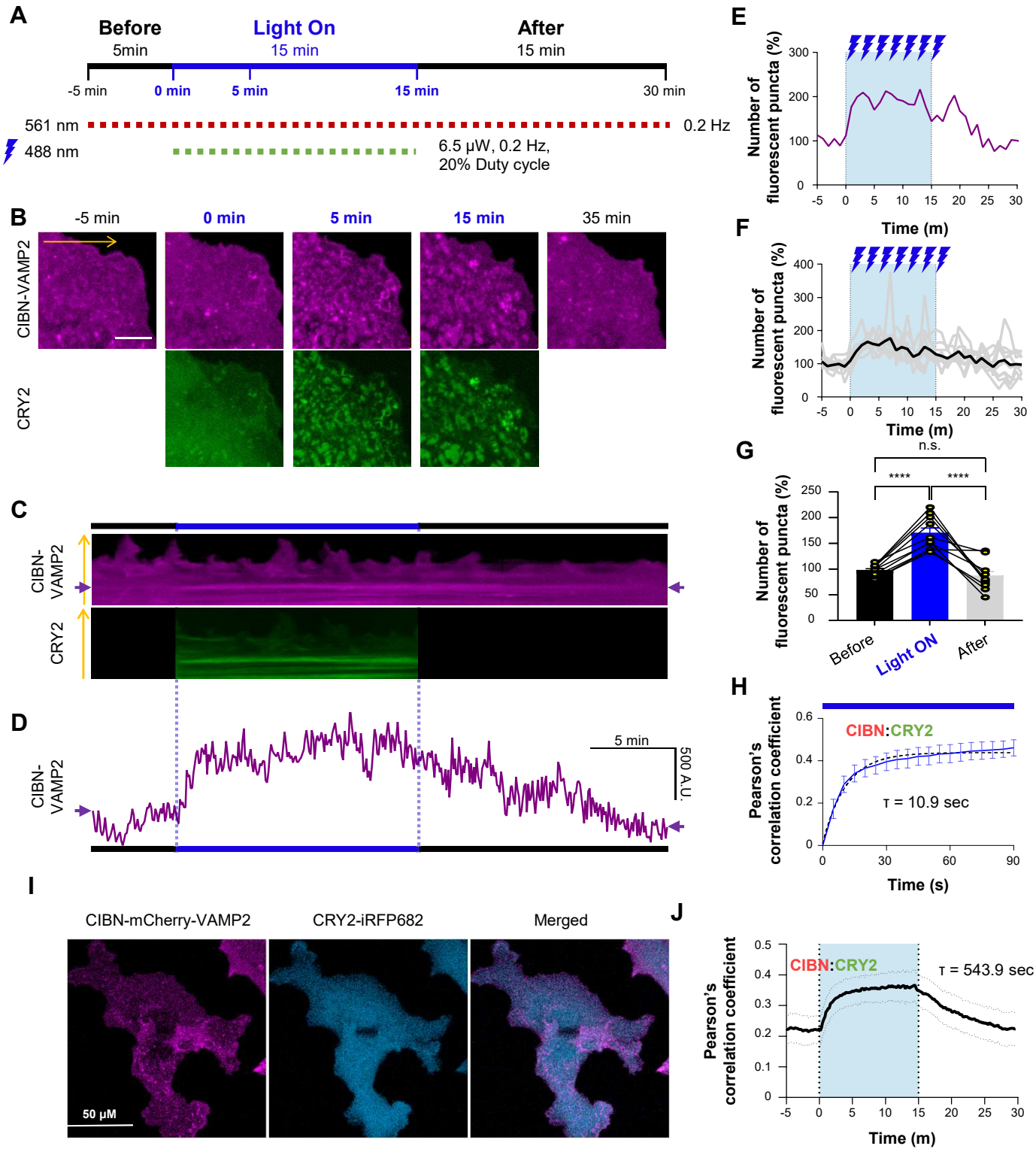

Figure 3: Optogenetic inhibition of vesicular exocytosis by Opto-vTtrap in Neuroscreen-1 cells.

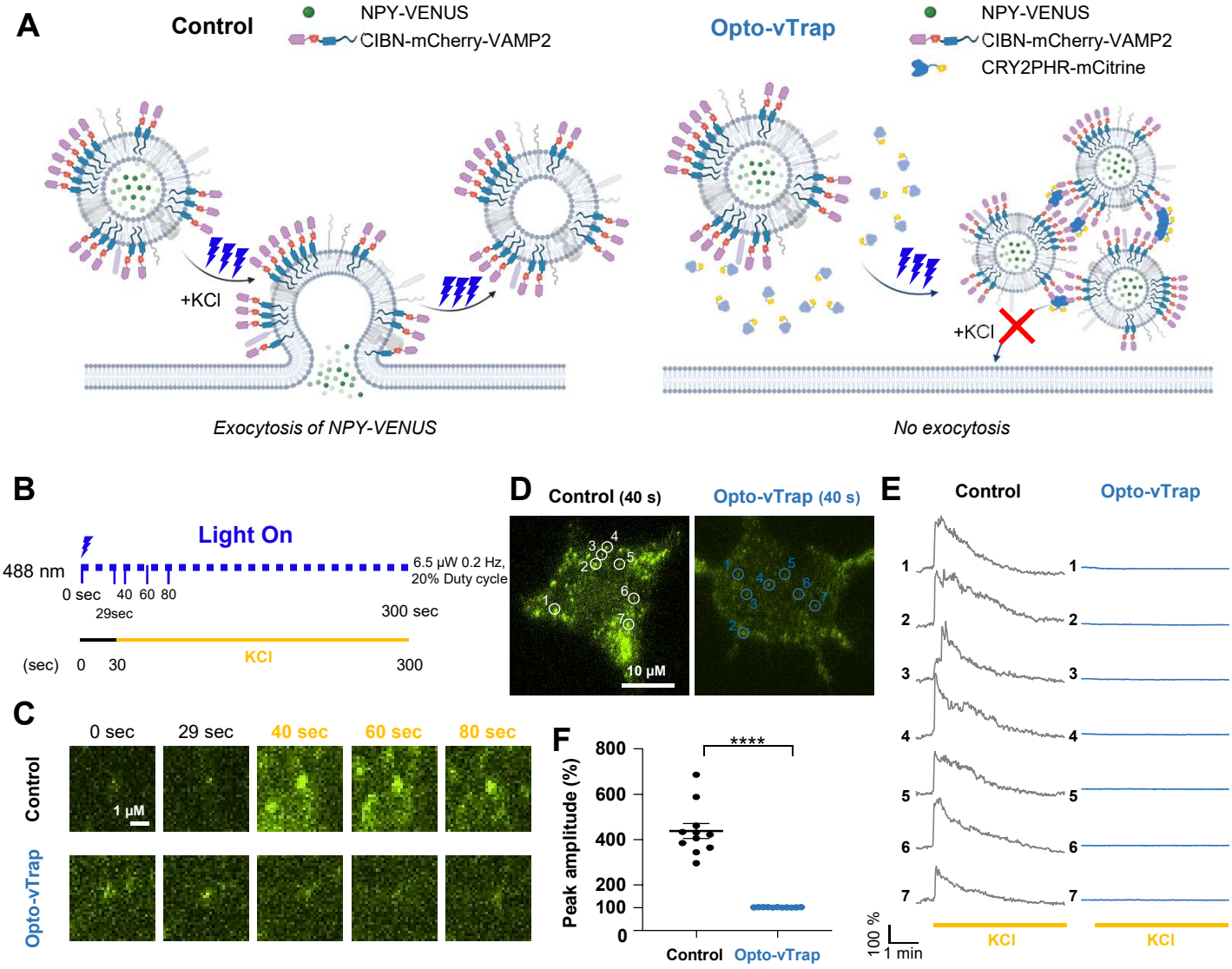

Figure 4: Activation of Opto-vTrap inhibits evoked EPSC in Schaffer-collateral synapses

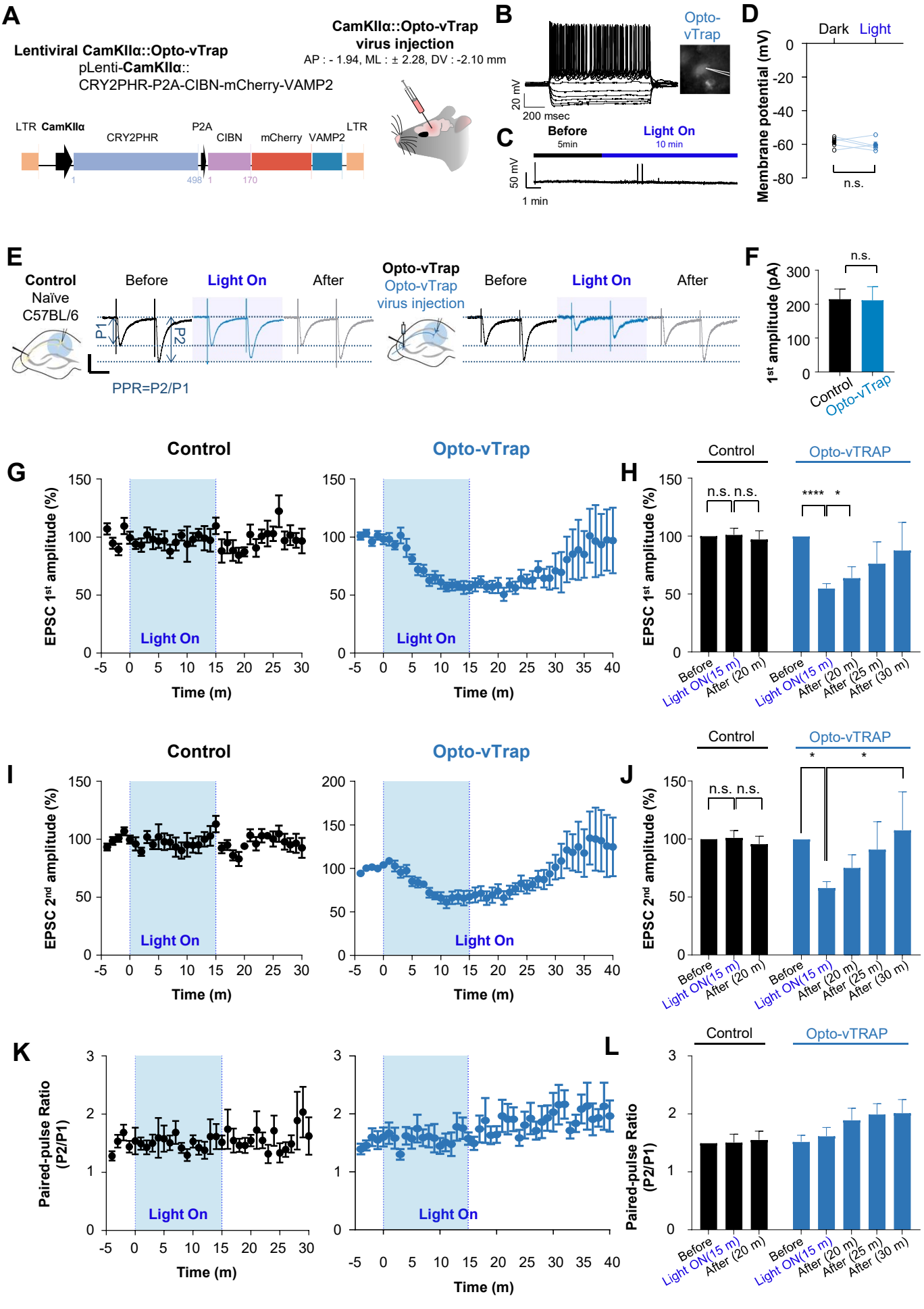

Figure 5: Activation of Opto-vTrap inhibits neocortical astrocytic vesicular gliotransmitter release

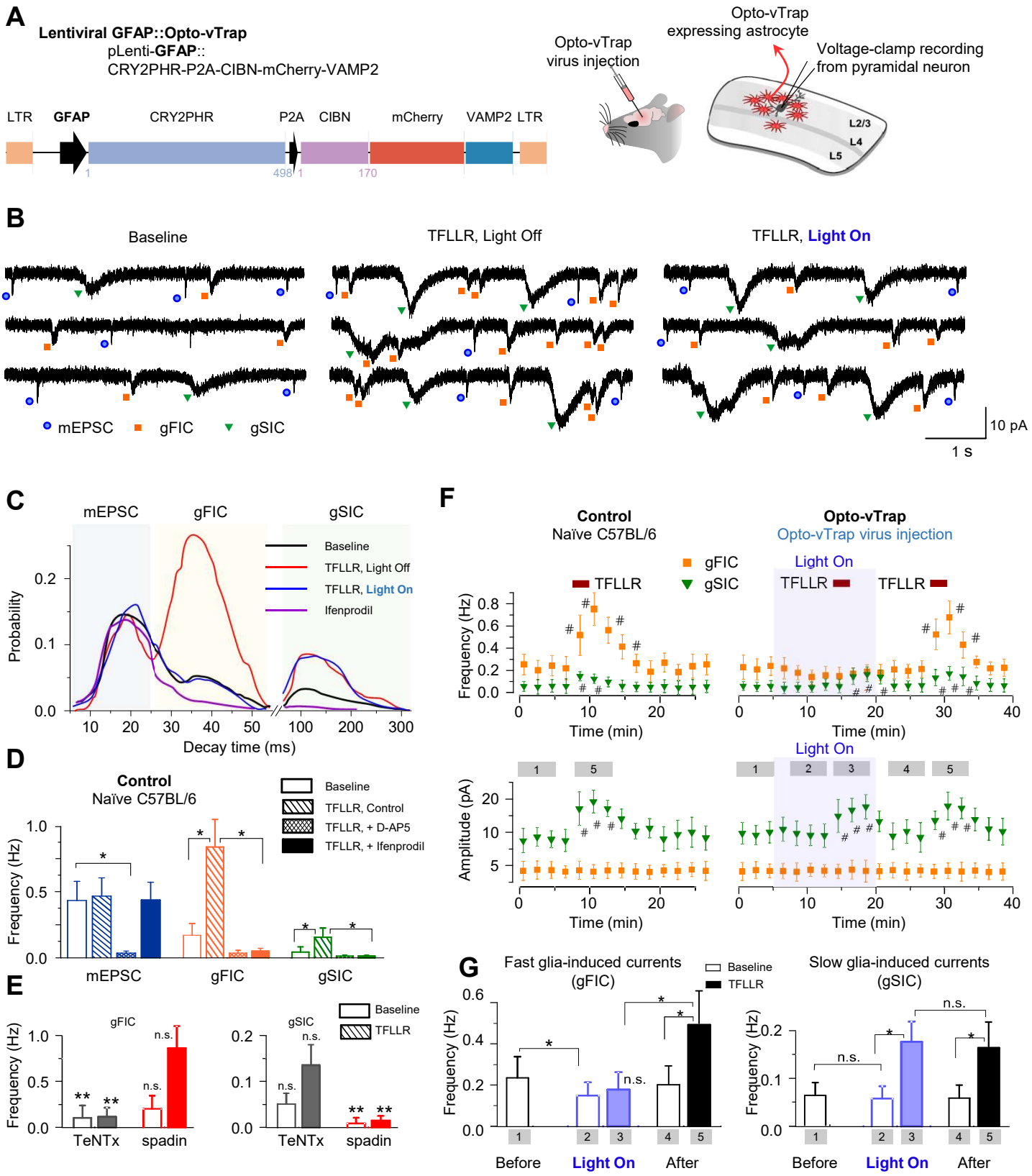

Figure 6: Activation of Opto-vTrap reversibly inhibits contextual fear memory retrieval